SUB-DOPPLER LASER SPECTROSCOPY OF H-2 AND D-2 IN THE RANGE 91-98 NM

Hinnen, P.C.; Hogervorst, W.; Stolte, S.; Ubachs, W.M.G.

published in
Canadian Journal of Physics
1994

DOI (link to publisher)
10.1139/p94-135

document version
Publisher's PDF, also known as Version of record

Sub-Doppler laser spectroscopy of H_2 and D_2 in the range 91–98 nm

P.C. HINNEN
Laser Centre Vrije Universiteit, Department of Physics and Astronomy, Department of Chemistry, DeBoelelaan 1081-1083, 1081 HV Amsterdam, The Netherlands

W. HOGERVORST
Laser Centre Vrije Universiteit, Department of Physics and Astronomy, DeBoelelaan 1081-1083, 1081 HV Amsterdam, The Netherlands

S. STOLTE
Laser Centre Vrije Universiteit, Department of Chemistry, DeBoelelaan 1081-1083, 1081 HV Amsterdam, The Netherlands

AND

W. UBACHS[1]
Laser Centre Vrije Universiteit, Department of Physics and Astronomy, DeBoelelaan 1081-1083, 1081 HV Amsterdam, The Netherlands

Received March 17, 1994
Accepted June 1, 1994

This paper is dedicated to Dr. Gerhard Herzberg on the occasion of his 90th birthday

The absorption spectra of hydrogen and deuterium have been measured in the range 91–98 nm. A narrowband extreme ultraviolet laser source is employed in combination with a molecular beam, allowing for sub-Doppler resolution and yielding linewidths of 0.23 cm^{-1}. Transition frequencies of 291 lines of the Lyman and Werner bands are determined with an average absolute accuracy of 0.03 cm^{-1}. The data are analyzed in a semi-empirical perturbation model, involving heterogeneous couplings between nearby lying levels of $B^1\Sigma_u^+$ and $C^1\Pi_u$ states. This model is found to be accurate on the level of accuracy of the data obtained.

Nous avons mesuré les spectres d'absorption de l'hydrogène et du deutérium, dans l'intervalle 91–98 nm, en utilisant une source laser à bande étroite dans l'extrême ultraviolet, en combinaison avec un faisceau moléculaire, ce qui a permis d'obtenir une résolution inférieure à l'effet Doppler et des largeurs de raie de 0,23 cm^{-1}. Les fréquences de 291 raies des bandes Lyman et Werner ont été déterminées avec une précision absolue moyenne de 0,03 cm^{-1}. Les données ont été analysées à l'aide d'un modèle semi-empirique de perturbations comportant des couplages hétérogènes entre niveaux voisins des états $B^1\Sigma_u^+$ et $C^1\Pi_u$. Ce modèle est suffisamment exact par rapport à la précision des données expérimentales.

[Traduit par la rédaction]

Can. J. Phys. 72, 1032 (1994)

1. Introduction

The hydrogen molecule has been the subject of innumerable spectroscopic investigations over the past 90 years. As a tribute to the pioneering observations of Lyman [1] and Werner [2], the $B^1\Sigma_u^-$–$X^1\Sigma_g^+$ and $C^1\Pi_u$–$X^1\Sigma_g^-$ electronic systems were named the Lyman and Werner bands. Since then many studies were performed with the goal of increasing the accuracy of the observations and of improving the analyses of these band spectra. References may be found in the data review of Huber and Herzberg [3].

Herzberg devoted a large part of his extensive scientific work to the understanding, unraveling, and accurate analysis of the spectrum of molecular hydrogen. The first high-resolution emission study of the Lyman bands was performed by Herzberg and Howe [4]. Herzberg was also involved in studies of the Rydberg states [5], and in a determination of the dissociation energy [6] and an analysis of the Lyman and Werner bands of HD [7] and D_2 [8, 9] isotopes. With the assignment of its Rydberg spectrum, he was the discoverer of triatomic neutral hydrogen [10]. His proposal of a possible quadrupole spectrum of molecular hydrogen [11] and its subsequent actual measurement [12] opened a new direction for experimental astronomy. Recently he has been involved in a study to accurately determine the ionization potentials of H_2 and D_2 [13, 14].

Here we present new high-resolution absorption data of the $B^1\Sigma_u^+$–$X^1\Sigma_g^+$ $(v', 0)$ $v' = 10$–19 and $C^1\Pi_u$–$X^1\Sigma_g^-$ $(v', 0)$ $v' = 2$–5 bands of H_2 and the $B^1\Sigma_u^-$–$X^1\Sigma_g^+$ $(v', 0)$ $v' = 14$–27 and $C^1\Pi_u$–$X^1\Sigma_g^+$ $(v', 0)$ $v' = 2$–7 bands of D_2 in the wavelength range 91–98 nm. The best existing absorption data for H_2 and D_2 in this wavelength range are those of Dabrowski and Herzberg [9] and to our knowledge no higher precision data have been obtained in the past 20 years. For the $B^1\Sigma_u^+$–$X^1\Sigma_g^-$ $(v', 0)$ $v' = 17$–19 and the $C^1\Pi_u$–$X^1\Sigma_g^+$ (5,0) bands of H_2 the even older data of Namioka [15] are still the most accurate. However, in the past decade the spectroscopy group of the Meudon Observatory has put considerable efforts into an accurate complete measurement of the emission spectrum of H_2 from a low-pressure discharge. These data have been published in the form of extensive tables for the Lyman [16] and Werner systems [17] and in the form of an atlas containing densitometer traces and a list with line identifications [18]. Along with the spectroscopic analyses of H_2 the Meudon group was also involved in calculations of rotational couplings between the Lyman and Werner systems [19]. These calculations are based on previous work by Julienne [20] and Ford [21]. Recently the calculations have been extended to incorporate the perturbing effects of the $B'^1\Sigma_u^+$ and $D^1\Pi_u$ states [22]. In these perturbation analyses use was made of ab initio potential energy and coupling strength calculations of

[1] Author to whom correspondence may be addressed.

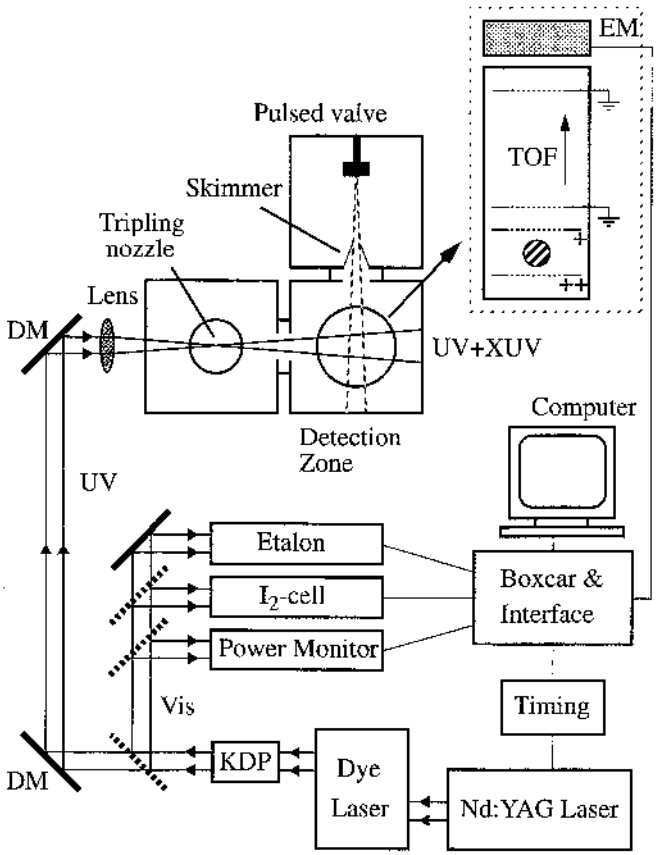

FIG. 1. Schematic of the experimental setup. DM: dichroic mirror. EM: electron multiplier. TOF: time-of-flight.

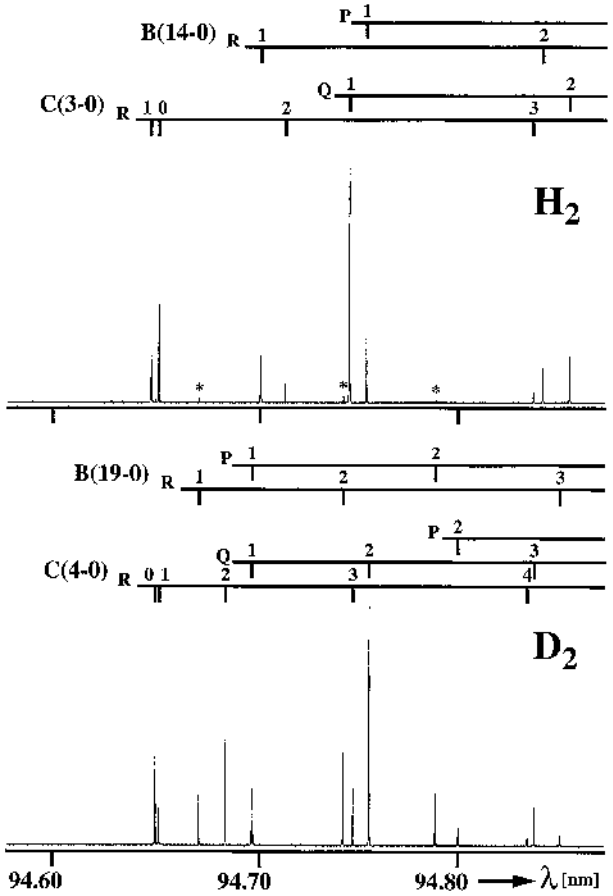

FIG. 2. Simultaneously recorded overview spectra of H_2 (upper) and D_2 (lower). Peaks in the H_2 spectrum marked with * are D^+ fragment ions coinciding with several D_2 resonances. Note that the order of the $R(0)$ and $R(1)$ lines of the $C^1\Pi_u$–$X^1\Sigma_g^+(3,0)$ band of H_2 is reversed as a result of strong interaction between the $C^1\Pi_u$, $v=3$ and $B^1\Sigma_u^+$, $v=14$ states.

Wolniewicz and Dressler [23] and of Senn et al. [24]. Based on these results many hitherto unassigned lines in the emission spectrum of H_2 could be identified [16, 17].

The present remeasurement of part of the absorption spectrum of hydrogen is motivated by the fact that, in particular, transitions involving the lowest J states of $X^1\Sigma_g^+$, $v=0$ are either missing or appearing as self-reversed lines in the H_2 atlas. In the present laser-based experiment the absolute calibration accuracy is better than in all previous work. The improved accuracy over data obtained by classical spectrographic techniques could be achieved by the use of a narrowband light source and an experimental configuration involving crossed laser and molecular beams allowing for sub-Doppler measurements. The transition frequencies in the extreme ultraviolet (XUV) are the exact sixth harmonic of visible frequencies, which may be compared to the I_2 absorption standard [25], thus providing an elegant calibration procedure. We note that accurate calibration of H_2 spectral lines is of astrophysical importance as well. H_2 absorption in the range 90–100 nm may act as a radiative shield preventing photo dissociation of the important CO molecule in interstellar clouds [26]. The Prasad-Tarafdar [27] cosmic-ray-induced XUV radiation model depends on coincidences between H_2 emissions and CO absorptions. In both cases accurate frequency calibration of the H_2 (and CO) transitions is of relevance. Of course a high-resolution spectroscopic investigation of the simplest molecule has an intrinsic value. Highly accurate determination of level energies may result, after comparison with theory, in values for radiative corrections in this system, analogous to the recent determination of the Lamb shift in atomic helium [28].

The spectroscopy of hydrogen received new impetus from recent developments in the field of powerful tunable and narrowband laser systems. To bridge the large gap between the electronic ground and excited states Eyler and co-workers used multi-photon techniques in combination with narrowband UV lasers for a study of the $E, F^1\Sigma_g^+$ states and for a subsequent determination of the ionization potential of H_2 and its isotopes [29–31]. With nonlinear optical conversion techniques, coherent radiation in the extreme ultraviolet below the lithium fluoride cutoff ($\lambda < 105$ nm) has become available for spectroscopy. An XUV laser source has been employed for an investigation of interference effects in the predissociation of hydrogen [32], while the technique of 1 XUV + 1 UV resonance-enhanced photoionization has been developed into a sensitive tool for the state-selective detection of hydrogen molecules [33–35]. Similarly XUV-laser-induced fluorescence has been found to be a powerful spectroscopic tool [36]. Recently a narrowband XUV laser was employed for an accurate determination of the dissociation limits of H_2, D_2, and HD [37–39].

The method of 1 XUV + 1 UV photoionization is applied here to record high resolution absorption spectra of Lyman and Werner bands of H_2 and D_2 in the range 91–98 nm. Transition

TABLE 1. Transition frequencies of the $B^1\Sigma_u^+$–$X^1\Sigma_g^+(v', 0)$ Lyman bands of H_2. The value in parentheses represents the uncertainty in the last digit. Δ_{oc} refers to the difference between present observations and the semi-empirical deperturbation calculation followed in the present work. Δ_1 refers to the difference between observations of ref. 9 for $v' \leq 16$ and of ref. 15 for $v' > 16$. Δ_2 refers to the deviation from ref. 16. All values in cm^{-1}

J	$R(J)$	Δ_{oc}	Δ_1	Δ_2	Band	$P(J)$	Δ_{oc}	Δ_1	Δ_2
					(10–0)				
0									
1	101 825.29 (2)	−0.01	†	−0.16§		101 746.48 (2)	+0.01	+0.33	−0.10‖
2	668.28 (2)	+0.01	+0.40	−0.16§					
					(11–0)				
0	102 882.16 (2)	+0.01	−0.16	−0.09§					
1	813.77 (2)	−0.01	−0.76*	−0.09§		102 738.55 (2)	−0.01	+0.34	−0.23‖,#
2	652.83 (2)	+0.00	−0.14	−0.11§					
					(12–0)				
0	103 844.62 (8)	−0.03	+0.06	+0.03 ,#					
1	776.75 (3)	+0.01	+0.27	−0.05§		103 701.17 (3)	+0.01	+0.26	+0.13‖
2	622.09 (7)	+0.00	‡	−0.05§,¶		490.25 (5)	−0.03	−0.24	−0.14‖
3	340.42 (3)	−0.00	‡	−0.04‖,#		189.71 (3)	−0.00	−0.28	+0.03‖
					(13–0)				
0	104 776.49 (3)	−0.03	+0.67*	−0.05‖					
1	704.87 (3)	−0.02	+0.19	−0.15§		104 634.65 (3)	+0.07	+0.55	+0.13§
2	539.13 (3)	+0.02	+0.19	−0.20§		422.11 (3)	−0.04	+0.24	+0.07 ,#
3	281.16 (3)	+0.01	+0.28	−0.00‖					
					(14–0)				
0	105 689.35 (4)	−0.03	‡	−0.09§					
1	598.93 (4)	+0.04	+0.75	+0.18‖		105 539.39 (3)	−0.00	†	−1.11#
2	432.92 (5)	−0.02	+0.14	−0.28§		335.02 (4)	+0.01	‡	+0.19#
3	172.55 (4)	+0.00	+0.12	+0.13‖,#					
					(15–0)				
0	106 556.69 (4)	−0.02	+0.02	−0.28§					
1	482.22 (3)	−0.01	−0.04	−0.25§		106 416.19 (4)	+0.01	+0.43	−0.13§
2	312.21 (3)	+0.01	+0.16	−0.27§		202.34 (3)	+0.01	+0.24	−0.61‖,#
3	048.57 (3)	−0.00	+0.17	−0.29§		105 895.20 (4)	+0.00	+0.11	+0.11
					(16–0)				
0	107 404.17 (3)	−0.03	+0.05	−0.35§					
1	326.95 (3)	+0.05	−0.00	+0.04 ,#		107 265.50 (5)	−0.08	+0.42	−0.16§
2	153.56 (3)	−0.03	+0.29	−0.42§		049.82 (3)	−0.01	+0.14	+0.14‖
3	106 886.00 (4)	−0.02	+0.18	−0.41§		106 739.91 (3)	+0.05	+0.29	+0.27‖
					(17–0)				
0	108 227.02 (3)	+0.02	+0.27	−0.23§					
1	149.94 (4)	+0.01	+0.09	−0.19§		108 087.76 (3)	−0.02	−0.13	−0.16§
2	107 976.05 (3)	−0.01	+0.43	−0.28§					
					(18–0)				
0	109 021.42 (6)	+0.08	−0.70	−0.14§					
1	108 941.81 (3)	−0.09	−0.38	−0.18§		108 883.52 (6)	+0.19	−0.24	−0.05§
2	764.51 (3)	−0.06	−0.89	−0.21§		666.99 (3)	+0.02	−0.08	−0.22§
3	491.67 (5)	+0.16	−0.21	−0.00§					
					(19–0)				
0	109 791.17 (3)	−0.05	−0.01	−0.06§					
1	711.88 (3)	+0.01	+0.32	+0.04§		109 653.24 (3)	+0.02	+0.27	+0.16§
2						436.94 (7)	+0.09	+0.57	+0.06§
3	264.40 (3)	−0.00	+0.34	+0.15§		124.85 (4)	+0.01	+0.41	+0.38‖

*Blended line, ref. 9.
†Overlapped by strong emission lines, ref. 9.
‡Misassignment, ref. 9.
§Not observed, calculated value, ref. 16.
‖Observed as self-reversed emission line, ref. 16.
¶Line observed more than 1 cm^{-1} away from calculated value, ref. 16.
#More than one assignment in emission spectrum, ref. 16.

frequencies are determined with an absolute accuracy ranging from 0.02 to 0.08 cm^{-1}. This is to be compared with an estimated absolute accuracy of 0.15 cm^{-1} in the work by Dabrowski and Herzberg [9] and of 1.5 cm^{-1} in the work of Namioka [15]. From a semi-empirical analysis, involving heterogeneous couplings between the $B^1\Sigma_u^+$ state and the $\Pi_{(c)}$ component of the $C^1\Pi_u$ state,

TABLE 2. Transition frequencies of the $C^1\Pi_u$–$X^1\Sigma_g^+(v', 0)$ Werner bands of H_2. The value in parentheses represents the uncertainties in the last digit. Δ_{oc} refers to the difference between present observations and the semi-empirical deperturbation calculation followed in the present work. Δ_1 refers to the difference between observations of ref. 9 for $2 \leq v' \leq 4$ and of ref. 15 for $v' = 5$. Δ_2 refers to the deviation from ref. 17. All values in cm^{-1}

J	$R(J)$	Δ_{oc}	Δ_1	Δ_2	$Q(J)$	Δ_{oc}	Δ_1	Δ_2	$P(J)$	Δ_{oc}	Δ_1	Δ_2
					(2–0) Band							
0	103 628.75 (3)	−0.03	+0.50*	−0.24§								
1	620.04 (3)	−0.00	+0.26	−0.27§	103 509.49 (3)	+0.00	+0.25	−0.14§				
2	541.68 (3)	+0.00	−0.14	−0.15‖	382.65 (6)	−0.01	−0.22	−0.14	103 274.44 (3)	+0.03	−0.09	+0.51‖,¶
3	436.16 (3)	+0.00	†	−0.20‖,¶	194.04 (4)	+0.00	−0.08	+0.04				
					(3–0) Band							
0	105 660.80 (3)	−0.00	†	−0.18§								
1	665.38 (3)	+0.02	+0.27	+0.07§	105 549.73 (3)	+0.02	‡	+0.12 ·¶				
2	584.26 (6)	−0.03	+0.28	+0.07‖	416.81 (3)	−0.04	+0.33**	+0.09 ·	105 306.40 (6)	+0.04	‡	−0.15‖,¶
3	438.64 (3)	+0.00	−0.15	+0.03‖	219.20 (3)	+0.02	+0.47	+0.16 ·	078.34 (3)	−0.03	+0.15	+0.14‖
					(4–0) Band							
0	107 580.95 (3)	−0.02	+0.12*	−0.08§								
1	562.99 (3)	+0.03	−0.10*	−0.01§	107 460.25 (3)	−0.02	−0.31	+0.20 ·				
2	475.24 (3)	+0.04	+0.13	−0.08‖	321.44 (3)	+0.04	−0.10	+0.22 ·,¶	107 226.54 (3)	−0.05	+0.10	−0.02‖
3	317.81 (4)	+0.00	−0.12	−0.26‖,¶	114.77 (3)	−0.02	+0.38	+0.07 ·	106 975.94 (4)	+0.01	−0.07	+0.08‖
4	090.40 (3)	−0.02	−0.03	−1.09¶	106 842.37 (4)	+0.01	+0.13	−0.10 ·¶	660.78 (3)	+0.00	+0.13	+0.70‖
					(5–0) Band							
0	109 361.70 (3)	−0.01	+0.13	−0.16§								
1	336.57 (4)	−0.01	−0.01	−0.19§	109 241.76 (6)	−0.04	+0.49*	+0.21 ·¶				
2	238.45 (3)	+0.01	+0.09	−0.21§	096.98 (3)	+0.02	+0.16	+0.10 ·¶	109 007.37 (4)	+0.03	+0.22	+0.14‖,¶
3	065.81 (5)	−0.01	−0.07	−0.27§	108 881.39 (4)	−0.02	−0.37	+0.36 ·	108 749.54 (3)	−0.01	+0.10	+0.25‖
4					597.12 (3)	+0.00	−0.68	+0.49 ·¶				

*Blended line, ref. 9 or ref. 15.
†Misassignment, ref. 9.
‡Not observed, ref. 9.
§Not observed, calculated value, ref. 17.
‖Observed as self-reversed emission line, ref. 17.
¶More than one assignment in emission spectrum, ref. 17.
**Overlapped by strong emission, ref. 9.

several reassignments of lines of H_2 by Abgrall et al. [16, 17] could be confirmed. For D_2 several lines, missing in the study of Dabrowski and Herzberg [9] due to overlap with emission lines of their XUV light source, were identified. The assignments of D_2 lines in the work of Dabrowski and Herzberg could be confirmed, with a few exceptions.

2. Experimental

The experimental setup and the performance of the XUV laser source have been described in some detail before [40] as well as its use in a preliminary study of the spectrum of H_2 [41]. In Fig. 1 the setup is schematically depicted. It consists of a dye laser pumped by an injection-seeded Nd:YAG laser. This system delivers, after frequency doubling in KDP, 4–6 mJ of tunable UV output in pulses of 4 ns duration. A molecular beam apparatus, composed of three interconnected and differentially pumped chambers, is used for the production of the XUV radiation, the formation of a skimmed probe-gas beam, and the detection of excited molecules. Because of the perpendicular alignment of laser and molecular beams, sub-Doppler measurements are possible. Tunable XUV light is obtained by third harmonic generation of the incident UV radiation focused (f = 15 cm) in a pulsed jet of xenon. The range 91–98 nm is covered while using Fluorescein-27, Rhodamine-6G, Rhodamine-B, and a mixture of the latter two in the dye laser. The timing of the laser pulse and the opening of the pulsed tripling and probe gas valves are synchronized. The tuning of the dye laser and the data acquisition are computer controlled.

Spectra of H_2 and D_2 are recorded by the highly sensitive technique of 1 XUV + 1 UV photoionization, i.e., the molecules are resonantly excited with XUV photons followed by ionization with nonresonant UV light. Ions are extracted from the interaction zone by a static electric field of 25 V cm^{-1}, mass-selected in a field-free time-of-flight (TOF) drift tube, and detected on an electron multiplier. Measurements are performed either on a pure H_2 molecular beam [41], but also simultaneous recording of H_2 and D_2 spectra is possible using a 50%/50% prepared mixture of H_2/D_2. Independent spectra of H_2 and D_2 are obtained by employing two boxcar integrators with gates set at the different arrival times of ion masses 2 and 4 at the detector. It should be noted that the XUV/UV laser beams diverge into the interaction region, where a sheet of 1 cm^2 crosses the molecular beam. Under these conditions no effects of 3 + 1 resonance-enhanced multi-photon ionization occur, as has been verified experimentally by switching off the XUV-producing tripling nozzle.

The wavelengths of the dye laser operating in the visible, the UV output, and the generated XUV are related as exact harmonics. Therefore the resonances observed in the XUV range may be calibrated by a reference spectrum at the fundamental

TABLE 3. Transition frequencies of the $B^1\Sigma_u^+ - X^1\Sigma_g^+(v', 0)$ Lyman bands of D_2. The value in parentheses represents the uncertainty in the last digit. Δ_{oc} refers to the difference between present observations and the semi-empirical deperturbation calculations followed in the present work. Δ_1 refers to the difference from observations of ref. 9. All values in cm^{-1}

J	$R(J)$	Δ_{oc}	Δ_1	Band	$P(J)$	Δ_{oc}	Δ_1
				(14–0)			
0	102 271.45 (3)	−0.02	+0.11				
1	238.35 (3)	+0.02	+0.12		102 198.37 (3)	+0.02	+0.13
2	158.92 (4)	+0.02	+0.12		092.38 (3)	−0.02	+0.14
				(15–0)			
0	102 981.79 (3)	+0.01	+0.13				
1	948.09 (3)	−0.01	+0.19		102 908.94 (3)	+0.01	‡
2	867.90 (3)	+0.00	+0.12		802.70 (3)	−0.01	+0.18
3					650.57 (3)	−0.00	+0.18
4	570.58 (3)	+0.00	+0.11		453.26 (3)	+0.01	+0.16
5	342.18 (8)	−0.00	+0.10				
				(16–0)			
0	103 677.05 (6)	+0.04	+0.14				
1	642.59 (3)	−0.02	+0.07		103 604.48 (7)	−0.04	+0.05
2	561.32 (3)	+0.02	+0.17		497.95 (3)	+0.01	+0.25
3	433.53 (4)	−0.02	+0.17		345.07 (3)	−0.00	+0.05
4	260.01 (3)	+0.00	+0.12		146.66 (3)	+0.00	+0.17
				(17–0)			
0	104 357.61 (5)	+0.01	+0.21				
1	322.92 (3)	+0.02	+0.24		104 285.31 (3)	+0.02	+0.10*
2	241.51 (6)	+0.02	+0.15		178.51 (3)	−0.02	+0.05
3					025.34 (3)	−0.03	+1.19*
4	103 933.23 (4)	−0.01	+0.15		103 286.92 (8)	+0.08	+0.20
5	714.33 (3)	+0.01	+0.02				
				(18–0)			
0	105 023.36 (3)	−0.03	−0.30				
1	104 987.84 (3)	+0.01	+0.11		104 951.52 (3)	+0.04	+0.08
2	904.81 (5)	+0.02	−0.00		844.28 (3)	−0.04	+0.05
3	774.69 (4)	−0.01	+0.00		690.32 (3)	+0.02	+0.07
4	598.21 (3)	+0.00	−0.05		490.15 (6)	+0.01	+0.14
				(19–0)			
0							
1	105 636.21 (3)	+0.03	+0.38		105 603.28 (3)	−0.02	+0.10*
2	553.20 (3)	−0.01	†		497.45 (3)	+0.02	†
3	422.24 (4)	+0.00	−0.08		338.62 (5)	−0.03	+0.03
4	244.50 (3)	+0.03	+0.07		138.54 (3)	−0.02	+0.10
5	020.84 (6)	−0.01	+0.06				
				(20–0)			
0	106 312.20 (3)	+0.02	+0.17				
1	275.52 (3)	+0.00	−0.44		106 240.79 (5)	−0.03	−0.04
2	190.83 (3)	+0.00	+0.04		133.08 (5)	−0.03	+0.37
3	058.54 (6)	−0.03	+0.05		105 977.99 (3)	+0.01	†
4	105 879.41 (3)	+0.00	+0.08		776.18 (4)	−0.00	+0.16
				(21–0)			
0	106 935.14 (3)	−0.05	+0.15				
1	897.74 (3)	+0.03	+0.23		106 864.31 (3)	+0.02	+0.00
2	811.98 (3)	+0.02	−0.08		756.13 (3)	+0.01	+0.13*
3	678.36 (3)	−0.06	m‡		600.25 (5)	+0.07	+0.04
4	497.72 (4)	−0.03	−0.33*		397.35 (3)	−0.05	−0.08
5	270.83 (3)	−0.02	+0.06				
				(22–0)			
0	107 544.77 (3)	−0.05	+0.22				
1	507.12 (3)	+0.02	+0.23		107 474.02 (3)	+0.02	+0.12
2	420.87 (3)	+0.03	+0.13		365.72 (3)	−0.04	−0.03
3	286.56 (4)	+0.04	+0.01		209.54 (5)	−0.03	−0.01
4	105.01 (3)	+0.06	+0.02		006.21 (5)	+0.02	−0.23
5	106 877.36 (3)	−0.07	−0.06				

TABLE 3. (*concluded*)

J	$R(J)$	Δ_{oc}	Δ_I	Band	$P(J)$	Δ_{oc}	Δ_I
				(23–0)			
0	108 140.52 (6)	+0.02	+0.14				
1	102.08 (3)	+0.02	+0.06		108 070.04 (3)	−0.01	+0.07
2	014.77 (3)	+0.02	−0.13		107 961.40 (6)	−0.03	+0.13
3							
4	107 695.84 (3)	+0.00	+0.20		600.06 (3)	−0.04	−0.03
				(24–0)			
0	108 722.77 (3)	−0.02	+0.29				
1	684.11 (3)	+0.00	+0.11		108 652.47 (3)	+0.00	+0.09
2	596.50 (3)	+0.01	+0.14		543.74 (4)	+0.02	+0.13
3	460.56 (7)	−0.02	+0.15				
				(25–0)			
0	109 291.66 (4)	+0.02	+0.26				
1	252.26 (4)	+0.00	+0.05		109 221.62 (3)	−0.03	+0.11
2	163.54 (3)	+0.02	+0.19		112.62 (3)	+0.05	+0.13
3	025.93 (4)	+0.01	+0.10		108 954.69 (3)	−0.04	+0.05
4	108 840.18 (3)	−0.00	+0.08		748.85 (4)	−0.02	+0.06
				(26–0)			
0	109 847.50 (5)	+0.03	+0.15				
1	807.97 (3)	−0.07	+0.03		109 777.54 (5)	+0.01	+0.04
2	719.44 (3)	+0.03	+0.13		668.49 (6)	+0.08	+0.05
3					510.51 (6)	+0.01	+0.17
4					304.80 (4)	+0.04	+0.16
				(27–0)			
0							
1							
2	110 259.64 (3)		+0.44		110 210.94 (3)		+0.35
3	120.12 (3)		‡				

*Blended line, ref. 9.
†Overlapped by strong emission lines, ref. 9.
‡Misassignment, ref. 9.

frequency. An iodine absorption spectrum [25] as well as the transmission fringes of an etalon (free spectral range 0.25 cm^{-1}) are recorded simultaneously with the XUV spectra. Line positions of hydrogen and deuterium are then determined by a computerized interpolation procedure, using selected and well-resolved I_2 lines. A correction for the I_2 standard is taken into account [42]. In a preliminary report [41] it was shown that the bandwidth of the XUV source could be reduced by using only the most coherent part of the dye laser beam. The observed width of the H_2 and D_2 resonances of 0.23(2) cm^{-1} (FWHM) is predominantly determined by the source bandwidth. Under the chosen condition of a nozzle-skimmer distance of 12 cm, the residual Doppler width, due to molecular and XUV-beam divergencies, is estimated to be 0.02 cm^{-1} for a pure H_2 beam, and below that value for mixed H_2/D_2 or H_2/Kr beams. The conditions in the interaction zone are essentially collision-free with densities on the order of 3×10^{10} particles/cm^3.

In a set of initial measurements on the (10,0) and (11,0) Lyman bands of H_2, data were collected with a step size of 0.005 cm^{-1} in the XUV. To correct for nonlinearities in the wavelength scan, using the equidistant markers of the etalon, frequency spans of 10 cm^{-1} in the XUV must be recorded around each resonance (see also ref. 41). By averaging 10 pulses per frequency position, while the system is running at 10 Hz, each recording of a line takes about 45 min. For the multiple recordings of the other 284 lines presented in this study the step size was increased to 0.025 cm^{-1} and the data averaging was decreased to 4 pulses per frequency setting. The price is a slight reduction in accuracy of the measured transition frequencies.

In sub-Doppler crossed-beam experiments a nonperfect perpendicular alignment will cause a systematic error in the frequency determination as a result of a Doppler shift. The angle between the molecular and laser beams is determined to be 88.5(3)° by aligning HeNe lasers along the beam paths. Moreover, the shift $\Delta\nu$ in a transition frequency ν_0 has been examined by changing the velocity of the molecules in the beam. This is accomplished by comparing the frequencies measured in a pure H_2 beam with those determined in a seeded beam of 20% H_2 in krypton. Through careful inspection of the statistics of multiple recordings a systematic shift in the absolute transition frequency of 0.01 cm^{-1} is found, which is in agreement with the measured angular misalignment. A similar procedure was followed in a determination of the absolute transition frequency of the resonance line of He near 58 nm in the same setup [28]. The results are consistent. From this analysis we deduce a systematic shift of 0.015 cm^{-1} for a pure H_2 beam and of 0.010 cm^{-1} for a mixed H_2/D_2 (50%/50%) beam. The transition frequencies reported in this paper are corrected for this net Doppler shift.

3. Results and analysis

Firstly, overview excitation spectra of H_2 and D_2 have been recorded in simultaneous measurements. In Fig. 2 an example is presented for the range 94.60–94.85 nm, showing Lyman

TABLE 4. Transition frequencies of the $C^1\Pi_u - X^1\Sigma_g^+(v', 0)$ Werner bands of D_2. The value in parentheses represents the uncertainty in the last digit. Δ_{oc} refers to the difference between present observations and the semi-empirical deperturbation calculation followed in the present work. Δ_1 refers to the difference from observations of ref. 9. All values in cm^{-1}

J	$R(J)$	Δ_{oc}	Δ_1	$Q(J)$	Δ_{oc}	Δ_1	$P(J)$	Δ_{oc}	Δ_1
				(2–0) Band					
0	102 678.00 (3)	−0.03	+0.44*						
1	675.84 (3)	+0.00	−0.17*	102 617.88 (3)	+0.00	+0.19			
2	642.62 (3)	+0.03	+0.08	555.57 (3)	−0.02	+0.22	102 498.98 (3)	+0.02	+0.16
3	578.32 (3)	−0.03	+0.13	462.56 (3)	+0.03	+0.15	378.30 (4)	−0.01	+0.05
4	482.90 (3)	+0.01	+0.19	339.14 (3)	−0.02	+0.03			
				(3–0) Band					
0	104 203.93 (3)	−0.00	+0.09						
1	199.38 (3)	−0.02	+0.03	104 143.81 (3)	−0.01	+0.03*			
2	162.32 (3)	−0.02	+0.04	079.39 (4)	+0.06	+0.22*	104 024.86 (3)	−0.01	+0.05*
3	089.08 (3)	+0.00	+0.24	103 983.01 (3)	−0.02	+0.03	103 901.93 (6)	+0.06	+0.17
4	103 998.61 (3)	−0.00	+0.15	855.38 (4)	−0.02	+0.11	747.73 (6)	+0.04	+0.10
5				697.09 (4)	+0.01	+0.15			
				(4–0) Band					
0	105 662.64 (4)	−0.01	−1.04*						
1	660.44 (3)	−0.01	+0.60	105 604.06 (3)	−0.01	+0.88*			
2	619.98 (3)	−0.01	+0.54	537.44 (3)	+0.01	†	105 483.59 (3)	+0.01	†
3	547.22 (3)	−0.00	†	437.89 (3)	+0.01	−0.03	362.93 (4)	+0.02	+0.08
4	441.88 (3)	+0.01	−0.16	305.93 (3)	−0.00	m‡	205.36 (3)	+0.02	+0.12
5	304.30 (5)	+0.04	m‡	142.20 (4)	−0.01	+0.09	017.29 (3)	−0.02	−0.55*
6	134.82 (6)	−0.03	+0.08	104 947.46 (3)	+0.01	−0.28			
				(5–0) Band					
0	107 059.44 (3)	−0.01	+1.03						
1	051.16 (3)	+0.04	+0.65	106 999.07 (3)	−0.04	−0.63			
2	008.59 (3)	+0.02	+0.26	930.48 (4)	+0.12	−1.88*	106 880.33 (3)	−0.05	+0.21
3	106 931.90 (3)	+0.01	−0.46*	827.65 (3)	−0.01	+0.07	753.60 (4)	+0.01	+0.13
4	821.26 (3)	−0.07	+0.32	691.46 (3)	−0.03	−0.08	593.97 (3)	+0.05	+0.15
5	676.93 (3)	+0.00	m‡	522.50 (3)	+0.01	+0.10	401.97 (3)	−0.01	−0.07
6				321.40 (6)	−0.01	−0.02			
				(6–0) Band					
0	108 389.81 (3)	−0.01	+0.12						
1	379.20 (4)	−0.00	+0.60	108 329.55 (7)	−0.01	+0.37			
2	333.29 (3)	+0.02	+0.16	258.70 (4)	−0.03	+0.31	108 210.75 (6)	−0.00	+0.10
3	252.00 (4)	−0.05	+0.17	152.91 (3)	+0.03	+0.03	081.67 (3)	+0.00	+0.03
4	135.38 (3)	+0.01	+0.38	012.49 (6)	−0.03	+0.09	107 918.63 (3)	+0.01	+0.17
5	107 981.01 (7)	−0.00	+0.13						
				(7–0) Band					
0	109 655.55 (3)	+0.00	+0.18						
1	642.58 (3)	+0.03	+0.16	109 595.39 (4)	−0.05	+0.29			
2	592.88 (3)	−0.01	+0.38	522.47 (3)	+0.03	−0.02	109 476.48 (3)	−0.00	+0.15
3	505.82 (3)	+0.02	−0.01	413.39 (4)	+0.01	−0.22	345.00 (3)	−0.02	+0.06
4	371.76 (3)	−0.00	+0.23	268.79 (4)	+0.03	−0.01	178.21 (5)	−0.03	−0.05
5	237.72 (5)	+0.00	+0.08	089.24 (4)	−0.01	+0.10			
6				108 875.61 (3)	−0.01	+0.13			

*Blended line, ref. 9.
†Overlapped by strong emission lines, ref. 9.
‡Misassignment, ref. 9.

and Werner band heads of both H_2 and D_2. The H_2 spectrum is contaminated by several weak lines that coincide with D_2 resonances. The D^+-fragmented ions, produced after XUV excitation of D_2, cannot be discriminated from the H_2^+ parent ion signals, produced in 1 XUV + 1 UV photoionization. Fragment ions, also produced at mass 1 after excitation of H_2, occur only at particular resonances and appear to have an uncorrelated intensity pattern. For example, the strongest line in the D_2 spectrum of Fig. 2, the $Q(2)$ line of the (4,0) Werner band, has no counterpart in the fragment-ion spectrum. Fragment ionization may be related to resonant excitation of doubly excited states, as well as to resonant photodissociation of H_2^+ and D_2^+. These processes were also observed after XUV excitation of HF and DF molecules [43]. The intensities observed in 1 XUV + 1 UV photoionization, producing H_2^+ and D_2^+ parent ions, do not follow ordinary Höhnl–London factors for rotational linestrengths. The UV-induced photoionization of excited B and C states depends on the occurrence of autoionization resonances, an effect that was investigated in some detail by Meier et al. [44]. As the intensity pattern does not provide a reliable tool for spectral identification, all line assignments are based on the measured transition frequencies.

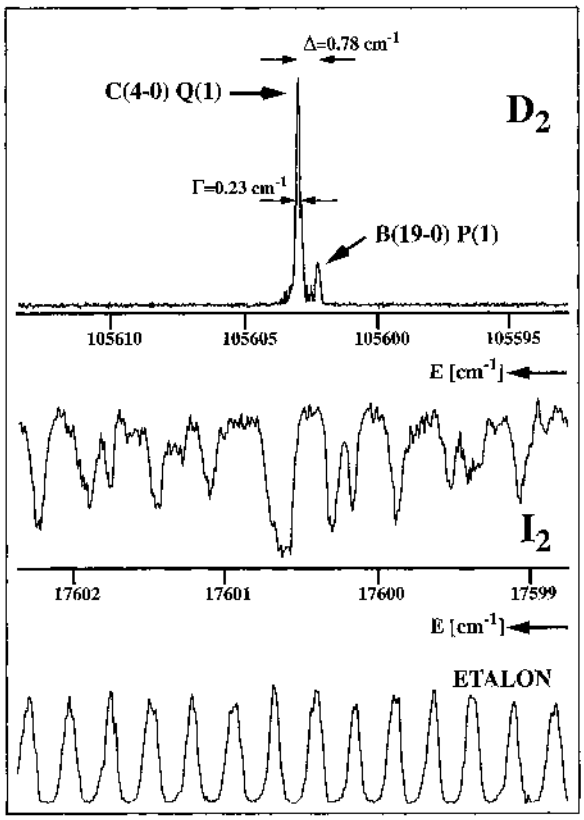

FIG. 3. Recording of two well-resolved D_2-resonances at 94.69 nm, which were blended in ref. 9. Also shown are the I_2 absorption spectrum (middle) and an etalon spectrum (lower), both used for calibration purposes.

TABLE 5. Band origin and rotational constants in the $B^1\Sigma_u^+$ state of H_2 as obtained from the fits. The value in parentheses represents the uncertainty in the last digit. All values in cm^{-1}

	Parameters fitted			Perturbing $C^1\Pi_u$ state	
v	ν_0	B_v	D_v	v	w_{BC}
10	101 864.97 (2)	13.067 (4)	0.0059 (2)	1	6.28*
11	102 857.04 (2)	12.562 (7)	0.0040 (5)		
12	103 819.65 (2)	12.218 (7)	0.0054 (4)	2	7.97 (2)
13	104 753.07 (4)	11.73 (1)	0.0027 (6)		
14	105 657.88 (3)	11.446 (4)	0.0052 (1)	3	9.28 (1)
15	106 534.67 (3)	11.024 (7)	0.0026 (3)		
16	107 384.07 (2)	10.807 (4)	0.006 (6)	4	11.3 (1)
17	108 206.27 (2)	10.278 (3)	0.0046 (6)	4	7.95 (5)
18	109 001.82 (2)	9.760 (3)	0.0*		
19	109 771.71 (2)	9.63 (1)	0.0*	5	7.4 (1)

*Value fixed in fitting procedure.

For the accurate calibration of H_2 and D_2 resonances, multiple recordings of large scans of at least 10 cm^{-1}, with a small frequency step size, have been taken. One example is given in Fig. 3, showing in a D_2 spectrum the experimental width of 0.23 cm^{-1}. Due to the high resolving power in the present sub-Doppler experiment the $Q(1)$ line of the (4,0) Werner band and the $P(1)$ line of the (19,0) Lyman band, which were blended in the work of Dabrowski and Herzberg [9], are now well resolved.

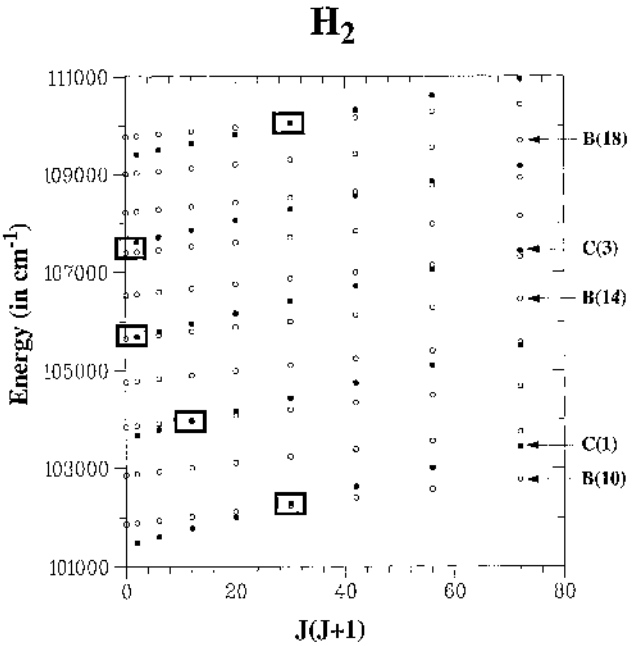

FIG. 4. Energy level diagram of the various ro-vibrational levels of the $B^1\Sigma_u^+$ (open dots) and $C^1\Pi_u$ (filled dots) electronic states of H_2. Local perturbations, that are incorporated in the perturbation analyses, are indicated by rectangular boxes.

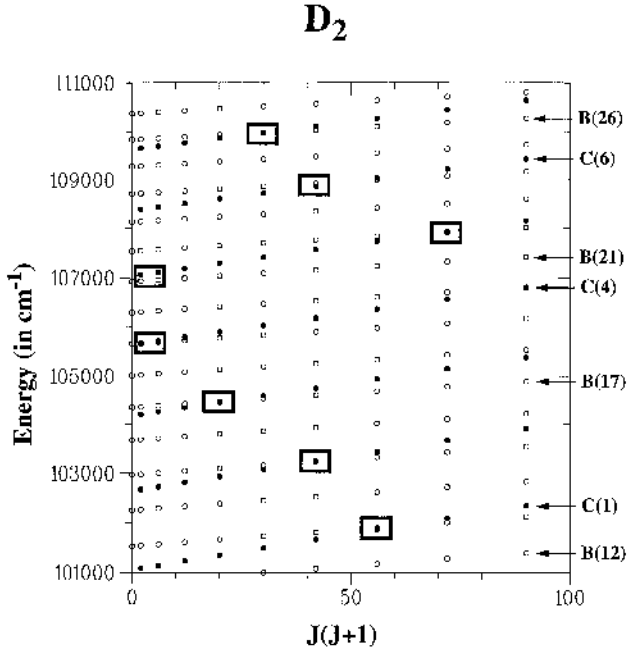

FIG. 5. Energy level diagram of the various ro-vibrational levels of the $B^1\Sigma_u^+$ (open dots) and $C^1\Pi_u$ (filled dots) electronic states of D_2. Local perturbations, which are incorporated in the perturbation analyses, are indicated by rectangular boxes.

In a preliminary report [41] it was explained that an absolute accuracy of 0.02 cm^{-1} in the transition frequency of some Lyman lines of H_2 can be achieved. In this value statistical errors as well as the inaccuracy of the I_2 standard are incorporated. The estimated error in the observed additional 284 lines is slightly

TABLE 6. Band origin and rotational constants in the $C^1\Pi_u$ state of H_2 as obtained from the fits. The value in parentheses represents the uncertainty in the last digit. All values in cm^{-1}

	$^1\Pi_u^-$			$^1\Pi_u^+$			Perturbing $B^1\Sigma_u^+$ state
	Parameters fitted			Parameters fitted			
v	ν_0	B_v	D_v	ν_0	B_v	D_v	v
2	103 600.62 (3)	27.371 (9)	0.0177 (5)	103 601.35 (2)	28.048 (3)	0.0235 (1)	12
3	105 642.35 (3)	25.862 (8)	0.0177 (4)	105 642.95 (4)	26.51 (1)	0.0252 (5)	14
4	107 554.42 (3)	24.356 (9)	0.0167 (5)	107 554.82 (3)	24.899 (4)	0.020 (2)	16, 17
5	109 337.44 (2)	22.860 (3)	0.0163 (1)	109 338.31 (3)	23.682 (9)	0.0313 (6)	19

TABLE 7. Band origin and rotational constants in the $B^1\Sigma_u^+$ state of D_2 as obtained from the fits. The value in parentheses represents the uncertainty in the last digit. All values in cm^{-1}

	Parameters fitted			Perturbing $C^1\Pi_u$ state	
v	ν_0	B_v	D_v	v	w_{BC}
14	102 258.13 (2)	6.674 (5)	0.001 7 (1)		
15	102 968.71 (2)	6.524 (4)	0.001 8 (1)	2	2.06 (1)
16	103 664.30 (3)	6.356 (5)	0.001 4 (1)		
17	104 345.07 (1)	6.224 (3)	0.001 72 (6)	3	2.61 (1)
18	105 011.26 (2)	6.068 (4)	0.001 5 (1)		
19	105 663.08 (2)	5.932 (4)	0.001 54 (9)	4	3.09 (1)
20	106 300.60 (3)	5.790 (5)	0.001 3 (1)		
21	106 924.07 (2)	5.656 (1)	0.001 3 (2)	5	3.44 (2)
22	107 533.78 (2)	5.498 (1)	0.001 6 (2)	5	3.62 (2)
23	108 129.83 (3)	5.337 (4)	0.000 4 (1)		
24	108 712.25 (2)	5.244 (3)	0.000 5 (2)	6	3.15 (4)
25	109 281.43 (2)	5.106 (4)	0.000 8 (1)		
26	109 837.31 (3)	5.024 (5)	0.001 5 (2)	7	3.38 (1)

larger, because of a larger frequency step size used and reduced statistical averaging. The measured transition frequencies and error margins are listed in Tables 1–4 for the Lyman and Werner bands of H_2 and D_2.

The ro-vibrational energy level structure of the $B^1\Sigma_u^+$ and $C^1\Pi_u$ states is known to deviate strongly from the simple functional forms as commonly found in diatomic molecules. Different models have been developed to account for the adiabatic as well as non-adiabatic corrections to the energy levels [20–24]. Here we chose to analyze the data in the form of a semi-empirical model involving rotational energy level series for the $B^1\Sigma_u^+$ and $C^1\Pi_u$ states, including heterogeneous perturbations between nearby vibrational levels. This procedure was also followed by Dabrowski and Herzberg [9]. As the lowest energy levels of other excited states of u-symmetry are all located above 110 000 cm^{-1}, effects of perturbing the $B'^1\Sigma_u^+$ and $D^1\Pi_u$ states may be left out of consideration. Excited level energies are expressed as:

$$E_v^B(J) = T_{ov}^B + B_v^B J(J+1) - D_v^B J^2(J+1)^2 \quad (1)$$

$$E_v^C(J) = T_{ov}^C + B_v^C[J(J+1) - \Lambda^2] - D_v^C[J(J+1) - \Lambda^2]^2 \quad (2)$$

where T_{ov} are the band origins, B_v and D_v are rotational constants, and Λ is taken as ± 1 for the $C^1\Pi$ state. For those vibronic states where a heterogeneous perturbation is expected, a J-dependent matrix of the form:

$$M(J) = \begin{bmatrix} E_v^B(J) & w_{BC}\sqrt{J(J+1)} \\ w_{BC}\sqrt{J(J+1)} & E_v^C(J) \end{bmatrix} \quad (3)$$

has been diagonalized for each value of J. Transition frequencies are calculated by subtracting rotational energies in the $X^1\Sigma_g^+$ ground state that were calculated with accuracies better than 0.01 cm^{-1} from molecular constants reported by Bragg et al. [45] for H_2 and by McKellar and Oka [46] for D_2. To identify mutually perturbing vibronic states, energy level diagrams are constructed for the $B^1\Sigma_u^+$ and $C^1\Pi_u$ states, based on the parameters of refs. 9 and 15. The diagram for H_2, shown in Fig. 4, covers the range of the presently observed vibronic states and is an extension of the diagram for the analysis of the emission spectrum constructed by Dabrowski [47]. The diagram for D_2 is shown in Fig. 5. In those cases, where the rotational energies of particular J states in $B^1\Sigma_u^+$ and $C^1\Pi_u$ approach closely, a perturbation treatment with a diagonalization of the energy matrix is performed. This is, for example, the case for $C^1\Pi_u$, $v = 2$ and $B^1\Sigma_u^+$, $v = 12$ of H_2 with a local perturbation near $J = 3$, or for $C^1\Pi_u$, $v = 3$ and $B^1\Sigma_u^+$, $v = 17$ of D_2 with a crossing near $J = 4$. In the particular example of the $B^1\Sigma_u^+$, $v = 21$ and $v = 22$ states of D_2, both states are found to be perturbed by the $C^1\Pi_u$, $v = 5$ state, and a 3×3 matrix has to be diagonalized. The same was done in H_2, where the $C^1\Pi_u$, $v = 4$ state undergoes local perturbations by $B^1\Sigma_u^+$, $v = 16$ and $v = 17$ levels. In other cases, for example, for the $B^1\Sigma_u^+$, $v = 11$ or $v = 15$ states of H_2, and the $B^1\Sigma_u^+$, $v = 16$ or $v = 18$ states of D_2, no perturbation treatment is necessary and the excited state energies can simply be expressed in the form of (1). In all cases the $C^1\Pi_u$, v states are incorporated in a perturbation analysis. All heterogeneous couplings incorporated in the analyses are indicated by rectangular boxes, which represent the local perturbations, in Figs. 4 and 5. It should be noted that only the Π_u^+-parity components of the C states, observed in the P and R lines, interact with the $^1\Sigma_u^+$ levels. The Π_u^- components, observed in the Q-lines, do not interact and are therefore expressed in the simple form of (2).

In separate least-squares minimization routines, either using a simple expression for a rotational sequence or a 2×2 or a 3×3 perturbation matrix, molecular constants are derived for all states presently investigated. The absorption data from refs. 9 and 15 are included in the fits, in so far as no remeasurements were performed. The transition frequencies of the Q-lines are used in separate fits and independent constants for the Π^- states are derived. Because of the high accuracy of the data obtained it became necessary to allow independent values for the band origins ν_0 in the fits of the Π^+ and Π^- levels. All data were weighted with appropriate errors in the fitting routines. The resulting values for the band origins, rotational constants, and

TABLE 8. Band origin and rotational constants in the $C^1\Pi_u$ state of D_2 as obtained from the fits. The value in parentheses represents the uncertainty in the last digit. All values in cm^{-1}

	$^1\Pi_u^-$			$^1\Pi_u^+$			
	Parameters fitted			Parameters fitted			Perturbing $B^1\Sigma_u^+$ state
v	ν_0	B_v	D_v	ν_0	B_v	D_v	v
2	102 663.39 (3)	14.277 (5)	0.004 9 (2)	102 663.61 (2)	14.447 (1)	0.005 35 (4)	15
3	104 189.88 (3)	13.725 (6)	0.004 3 (2)	104 190.12 (2)	13.904 (8)	0.005 1 (3)	17
4	105 650.67 (3)	13.187 (3)	0.004 35 (8)	105 650.84 (2)	13.374 (3)	0.005 42 (5)	19
5	107 046.24 (6)	12.660 (7)	0.004 4 (2)	107 046.46 (2)	12.853 (1)	0.004 6 (5)	21, 22
6	108 377.21 (5)	12.139 (6)	0.004 5 (1)	108 377.52 (3)	12.359 (4)	0.005 6 (2)	24
7	109 643.63 (3)	11.596 (3)	0.004 10 (7)	109 643.87 (2)	11.802 (4)	0.005 28 (9)	26

perturbation parameters are listed in Tables 5–8. The calculated transition frequencies, following from these procedures, are compared with the observed values, and the deviations are included in Tables 1–4. The listed values show that the deviations fall within the estimated experimental error margins, thus supporting the validity of the semi-empirical model. Perturbative shifts of up to 15 cm^{-1} are involved, which in the deperturbation model can be accounted for within the accuracy of 0.03 cm^{-1}.

On the basis of the present analysis the assignment of seven lines for H_2 has to be revised with respect to ref. 9. In the work of the Meudon group most of the lines involving low J could not be observed. However, this group calculated transition frequencies for the low J states from an analysis of the emission spectrum. The deviations from these calculations, also listed in Tables 1 and 2, are found to be small. Moreover, the reassignments of the H_2 lines in refs. 16 and 17 in the Lyman and Werner bands could be confirmed in the present analysis. For D_2 only the work of Dabrowski and Herzberg is available for comparison. All their assignments are confirmed, apart from an interchange of the $R(5)$ and $Q(4)$ lines of the (4,0) Werner band and the $B(21,0)$ $R(3)$ and $C(5,0)$ $R(5)$ lines.

4. Conclusion

In the present study transition frequencies of 291 rotationally resolved absorption lines in the Lyman and Werner band systems of molecular hydrogen and deuterium have been measured with an absolute accuracy ranging from 0.02 to 0.08 cm^{-1}. This is a considerable improvement over previous studies. A semi-empirical deperturbation analysis, which is valid on the level of accuracy of the present data, has been performed. From this analysis accurate values for the molecular constants are derived. We note that the present model includes only the effects of local perturbations, which give rise to non-adiabatic fluctuation shifts [20]. It is a simplification in so far as a smooth background shift, caused by interactions with all v-levels of the $B^1\Sigma_u^+$ state and its continuum, is not regarded.

The values for the band origins of the Lyman bands may be of importance for comparison with future ab initio calculations. The energies of $B^1\Sigma_u^+$, $v = 0$, $J = 0$ levels of both H_2 and D_2 are determined with a precision of 0.01–0.03 cm^{-1}, as can be deduced from the consistency of the fits. It should be noted here that the absolute calibration of the I_2 standard, used as a reference in the present investigation, is 0.001 cm^{-1} (1 σ error [42]). Consequently the systematic calibration error of the XUV resonances in the present study is 0.006 cm^{-1}. As the rotationless levels are not affected by heterogeneous couplings to the $^1\Pi$ levels, the $J = 0$ states may therefore be calculated more accurately than the $J \neq 0$ states. A precise determination of the potential energy minimum of the $B^1\Sigma_u^+$ state, from which radiative corrections may be derived, must, however, await new measurements of the low v levels.

Because of the high absolute accuracy of the measured transition frequencies many of these lines can in future be used for calibration purposes in the XUV domain. We are in the process of replacing the dye laser, which is the bandwidth limiting part of our XUV laser source, by a pulsed dye amplification system. With this device an increase of resolution may be obtained, thus providing an opportunity to perform even higher resolution studies on H_2 and D_2.

Acknowledgements

The authors wish to thank J. Bouma for his excellent technical support. A special (USF-project) grant by the Vrije Universiteit Amsterdam is gratefully acknowledged.

1. Th. Lyman. Astrophys. J. **23**, 181 (1906).
2. S. Werner. Proc. R. Soc. London, A, **113**, 107 (1926).
3. K.P. Huber and G. Herzberg. Molecular spectra and molecular structure IV. Constants of diatomic molecules. Van Nostrand–Reinhold, New York. 1979.
4. G. Herzberg and L.L. Howe. Can. J. Phys. **37**, 636 (1959).
5. G. Herzberg and Ch. Jungen. J. Mol. Spectrosc. **41**, 425 (1972).
6. G. Herzberg. J. Mol. Spectrosc. **33**, 147 (1970).
7. I. Dabrowski and G. Herzberg. Can. J. Phys. **54**, 525 (1976).
8. H. Bredohl and G. Herzberg. Can. J. Phys. **51**, 867 (1973).
9. I. Dabrowski and G. Herzberg. Can. J. Phys. **52**, 1110 (1974).
10. G. Herzberg. J. Chem. Phys. **70**, 4806 (1979).
11. G. Herzberg. Astrophys. J. **87**, 428 (1938).
12. G. Herzberg. Nature, **163**, 170 (1949).
13. Ch. Jungen, I. Dabrowski, G. Herzberg, and M. Vervloet. J. Chem. Phys. **93**, 2289 (1990).
14. Ch. Jungen, I. Dabrowski, G. Herzberg, and M. Vervloet. J. Mol. Spectrosc. **153**, 11 (1992).
15. T. Namioka. J. Chem. Phys. **40**, 3154 (1964).
16. H. Abgrall, E. Roueff, F. Launay, J.Y. Roncin, and J.L. Subtil. Astron. Astrophys. Suppl. Ser. **101**, 273 (1993).
17. H. Abgrall, E. Roueff, F. Launay, J.Y. Roncin, and J.L. Subtil. Astron. Astrophys. Suppl. Ser. **101**, 323 (1993).
18. J.Y. Roncin and F. Launay. J. Phys. Chem. Ref. Data Monogr. 4. In press.
19. H. Abgrall, E. Roueff, F. Launay, J.Y. Roncin, and J.L. Subtil. J. Chem. Phys. **87**, 2036 (1987).
20. P.S. Julienne. J. Mol. Spectrosc. **48**, 508 (1973).
21. A.L. Ford. J. Mol. Spectrosc. **56**, 251 (1975).
22. H. Abgrall, E. Roueff, F. Launay, J.Y. Roncin, and J.L. Subtil. J. Mol. Spectrosc. **157**, 512 (1993).

23. L. Wolniewicz and K. Dressler. J. Chem. Phys. **88**, 4720 (1988).
24. P. Senn, P. Quadrelli, and K. Dressler. J. Chem. Phys. **89**, 7401 (1988).
25. S. Gerstenkorn and P. Luc. Atlas du spectre d'absorption de la molecule d'iode. CNRS, Paris. 1978.
26. E.F. van Dishoeck and J.H. Black. Astrophys. J. **334**, 771 (1988).
27. S.S. Prasad and S.P. Tarafdar. Astrophys. J. **267**, 603 (1983).
28. K.S.E. Eikema, W. Ubachs, W. Vassen, and W. Hogervorst. Phys. Rev. Lett. **68**, 1690 (1993).
29. E.E. Eyler, J. Gilligan, E. McCormack, A. Nussenzweig, and E. Pollack. Phys. Rev. A: Gen. Phys. **36**, 3486 (1987).
30. E. McCormack, J.M. Gilligan, C. Corniggia, and E.E. Eyler. Phys. Rev. A: Gen. Phys. **39**, 2260 (1989).
31. J.M. Gilligan and E.E. Eyler. Phys. Rev. A: Gen. Phys. **46**, 3676 (1992).
32. M. Rotschild, H. Egger, R.T. Hawkins, H. Pummer, and C.K. Rhodes. Chem. Phys. Lett. **72**, 404 (1980).
33. E.E. Marinero, C.T. Rettner, R.N. Zare, and A.H. Kung. Chem. Phys. Lett. **95**, 486 (1983).
34. H. Rottke and K.H. Welge. Chem. Phys. Lett. **99**, 4536 (1983).
35. A.H. Kung, T. Trickl, N.A. Gershenfeld, and Y.T. Lee. Chem. Phys. Lett. **144**, 427 (1988).
36. F.J. Northrup, J.C. Polanyi, S.C. Wallace, and J.M. Williamson. Chem. Phys. Lett. **105**, 34 (1984).
37. A. Balakrishnan, V. Smith, and B.P. Stoicheff. Phys. Rev. Lett. **68**, 2149 (1992).
38. A. Balakrishnan and B.P. Stoicheff. J. Mol. Spectrosc. **156**, 517 (1992).
39. A. Balakrishnan, M. Vallet, and B.P. Stoicheff. J. Mol. Spectrosc. **162**, 168 (1993).
40. W. Ubachs. K.S.E. Eikema, and W. Hogervorst. Appl. Phys. B, **57**, 411 (1993).
41. P.C. Hinnen, W. Hogervorst, S. Stolte, and W. Ubachs. Appl. Phys. B, **59**, 307 (1994).
42. S. Gerstenkorn and P. Luc. Rev. Phys. Appl. **14**, 791 (1979).
43. L.M. Tashiro, W. Ubachs, and R.N. Zare. J. Mol. Spectrosc. **138**, 89 (1989).
44. W. Meier, H. Rottke, H. Zacharias, and K.H. Welge. J. Chem. Phys. **83**, 4360 (1985).
45. S.L. Bragg, J.W. Brault, and W.H. Smith. Astrophys. J. **263**, 999 (1982).
46. A.R.W. McKellar and T. Oka. Can. J. Phys. **56**, 1315 (1978).
47. I. Dabrowski. Can. J. Phys. **62**, 1639 (1984).